Real time path integrals using the Herman–Kluk propagator

John C. Burant and Victor S. Batista
Department of Chemistry, Yale University, New Haven, Connecticut 06520-8107

(Received 18 October 2001; accepted 27 November 2001)

It is shown that the accuracy of quantum dynamics calculations obtained according to the Herman–Kluk (HK) semiclassical initial value representation (SC-IVR) is significantly improved when the time evolution operator is computed by concatenating finite time propagators. This approach results in an approximate calculation of a real-time path-integral in a discrete coherent-state representation, which becomes exact in the limit of sufficiently short time-slice intervals. The efficiency of the computational method is optimized by devising a compact coherent-state basis set that obviates the need for calculating the inverse overlap matrix. Quantitative agreement with full quantum mechanical results is verified in the description of tunneling between disjoint classically allowed regions in one- and two-dimensional systems, in the treatment of long-time dynamics, and in nonadiabatic dynamics in a model system with two coupled one-dimensional potential energy surfaces. © *2002 American Institute of Physics.* [DOI: 10.1063/1.1436306]

I. INTRODUCTION

Understanding quantum mechanical effects in the evolution of chemical reactions is a fundamental problem of much current research interest in chemical dynamics. This requires, at the most fundamental level of theory, solving the time-dependent Schrödinger equation. Not surprisingly, much effort has been devoted to the development of rigorous computational methods for directly solving this equation. Exact quantum mechanical calculations usually require storage of multidimensional wave functions and computational effort that grows exponentially with the number of coupled degrees of freedom. These methods are therefore feasible for systems with only a few degrees of freedom and they are likely to remain of limited applicability, even with projected advances in computer technology. It is, therefore, essential to develop approximate computational methods of useful reliability for describing the most basic forms of quantum phenomena (e.g., interference and tunneling). In this paper we develop one such method by implementing the Herman–Kluk (HK) semiclassical initial value representation[1] (SC-IVR) according to a time-slicing technique.

SC-IVR methods originated more than 30 years ago[2] as a practical way of incorporating quantum effects into classical molecular dynamics simulations. In recent years, there has been considerable interest in the development of new SC-IVR implementation methods. The ultimate goal has been to establish truly convenient alternatives to full-quantum mechanical techniques.[3] The new implementation methodologies have been successfully implemented not only in a number of model test systems,[4–13] but also in simulations of realistic reactions that allowed for direct comparisons with experimental data.[14–17] Some of the applications to real photodissociation reactions provided an intuitive understanding of the most fundamental dynamical features involved in electronic nonadiabatic processes of interconversion, as well as first principle interpretations of the total photoabsorption cross section as a function of the photolysis wavelength.[17] SC-IVR techniques have been applied to simulations of realistic two-color pump–probe experiments of femtosecond photoelectron spectroscopy,[18] simulations of ultrafast photoinduced proton transfer reactions,[19,20] and simulations of coherent-control.[21,22]

Unfortunately, however, all SC-IVR methods are slowly convergent in the treatment of long time dynamics and encounter serious difficulties in the description of tunneling between disjoint classically allowed regions (i.e., deep tunneling). These methods usually require an enormous number of trajectories to achieve accurate results at long times, since the integral over the initial phase space results in poor Monte Carlo (MC) statistics. The integrand usually becomes highly oscillatory at long times and gives rise to phase cancellation problems similar to those encountered in full quantum path integral techniques. This problem, which is already present for one-dimensional systems, usually becomes far more serious in multidimensional systems with chaotic classical dynamics. Several techniques have been proposed to overcome the numerical difficulties, including methods that simply discard trajectories when they become problematic,[23] rigorous filtering techniques based on stationary phase MC integral conditioning methods,[9,10,17,24–30] linearized approximations,[31–34] forward–backward techniques,[18,35,36] and the time-integrated form.[37] Unfortunately, however, this problem still constitutes a serious obstacle for general purpose applications. Furthermore, SC-IVR methods encounter serious difficulties in the treatment of deep tunneling[12,38–40] even at fairly short propagation times. This is one of the most basic forms of quantum phenomena and is vital in the description of chemical reactions and molecular spectroscopy.[41–45]

Since SC-IVR methods have been extremely successful for describing quantum effects in the short time dynamics of polyatomic systems without deep tunneling, it is natural to try to extend such approaches and develop methods that build upon the SC-IVR while offering improved accuracy. The goal of this paper is to develop an implementation of the HK SC-IVR that is free of convergence problems in the

treatment of long time dynamics and is of useful reliability for the description of deep tunneling. The resulting computational approach bridges the gap between semiclassical and full quantum dynamics by implementing the semiclassical propagator for finite time intervals along the lines of previous proposals.[12,46,47] The algorithm becomes an exact path integral calculation in a coherent-state representation when the finite time intervals become infinitesimally short.

The approach implemented in this paper is computationally more efficient than a standard Feynman path integral calculation.[48] The method avoids the exponential proliferation of trajectories by computing individual trajectories for finite propagation times and subsequently initializing new trajectories according to the time evolved wave function. The semiclassical propagator[2,49,50] allows for time slices that are longer than the infinitesimal time slices required by the free particle propagator. In the past, numerical problems associated with the proliferation of trajectories have limited the applicability of the Feynman path integral approach to one-dimensional model systems, despite extensive work dedicated to overcome the underlying numerical difficulties.[24,51,52]

The paper is organized as follows: Section II describes the methodology. Section III details the application of the method to one- and two-dimensional double-well tunneling problems and discusses the improvement relative to the standard HK SC-IVR method. Section IV discusses how this formalism can be implemented for simulating quantum dynamics on coupled potential energy surfaces and illustrates the approach for a simple curve-crossing model system. Section V discusses our results and the possible extension to larger systems. Finally, Sec. VI summarizes and concludes.

II. FORMULATION OF THE TIME-SLICED PROPAGATOR

Matrix elements of the quantum mechanical propagator,

$$K(\mathbf{x}_n,t_n|\mathbf{x}_0,t_0)=\langle \mathbf{x}_n|e^{-i\hat{H}(t_n-t_0)/\hbar}|\mathbf{x}_0\rangle \tag{1}$$

can be time-sliced (TS) by repeatedly inserting the resolution of identity,

$$\hat{1}=\int \mathbf{dx}|\mathbf{x}\rangle\langle\mathbf{x}| \tag{2}$$

yielding

$$\begin{aligned}\langle \mathbf{x}_n|e^{-i\hat{H}(t_n-t_0)/\hbar}|\mathbf{x}_0\rangle &= \int d\mathbf{x}_{n-1}\cdots\int d\mathbf{x}_1\langle \mathbf{x}_n|e^{-(i/\hbar)\hat{H}(t_n-t_{n-1})}|\mathbf{x}_{n-1}\rangle \\ &\cdots\langle \mathbf{x}_1|e^{-(i/\hbar)\hat{H}(t_1-t_0)}|\mathbf{x}_0\rangle,\end{aligned} \tag{3}$$

where $t_0<t_1<\cdots<t_{n-1}<t_n$. For sufficiently short time periods, $\tau=t_k-t_{k-1}$, each propagator introduced by Eq. (3) can be well approximated by the semiclassical propagator in its coherent-state representation,[1]

$$\begin{aligned}e^{-(i/\hbar)\hat{H}\tau}\approx(2\pi\hbar)^{-D}\int \mathbf{dp}_0\int \mathbf{dq}_0|\mathbf{p}_\tau\mathbf{q}_\tau\rangle \\ \times C_\tau(\mathbf{p}_0\mathbf{q}_0)e^{iS_\tau(\mathbf{p}_0,\mathbf{q}_0)/\hbar}\langle \mathbf{p}_0,\mathbf{q}_0|,\end{aligned} \tag{4}$$

where $|\mathbf{p}_\tau\mathbf{q}_\tau\rangle$ are the minimum uncertainty wave packets, or coherent states (CS),

$$\langle \mathbf{x}|\mathbf{p}_\tau\mathbf{q}_\tau\rangle=\left(\frac{2\gamma}{\pi}\right)^{D/4}\exp[-\gamma(\mathbf{x}-\mathbf{q}_\tau)^2+i\mathbf{p}_\tau(\mathbf{x}-\mathbf{q}_\tau)/\hbar]. \tag{5}$$

The constant parameter γ introduced by Eq. (5) is the width of the coherent state. The integration variables $(\mathbf{p}_0,\mathbf{q}_0)$ in Eq. (4) are the initial conditions for classical trajectories of the time-evolved coordinates and momenta $\mathbf{q}_\tau\equiv\mathbf{q}_\tau(\mathbf{p}_0,\mathbf{q}_0)$ and $\mathbf{p}_\tau\equiv\mathbf{p}_\tau(\mathbf{p}_0,\mathbf{q}_0)$, obtained by integrating the usual classical equations of motion. $S_\tau(\mathbf{p}_0,\mathbf{q}_0)$ is the classical action along this trajectory, obtained by integrating the equation

$$\dot{S}_t=\mathbf{p}_t\cdot\dot{\mathbf{q}}_t-H(\mathbf{p}_t,\mathbf{q}_t), \tag{6}$$

for time τ. Finally, the pre-exponential factor $C_\tau(\mathbf{p}_0,\mathbf{q}_0)$ in Eq. (4) involves the monodromy matrix elements that are propagated according to the equations for the stability matrix.[1]

Details of the standard implementation of the HK propagator are readily available in the literature[1,12,13,53] and will not be discussed here. The time-slicing procedure, described in this paper, improves upon that standard implementation and approaches the full quantum propagator in the $\tau\to 0$ limit.[54] This limit has been previously considered within the context of the SC-IVR.[46,55] This paper shows for the first time that it can actually be reached in practice.

For $\tau=0$, Eq. (4) gives an exact representation of unity in the nonorthogonal CS basis,[56]

$$\hat{1}=(2\pi\hbar)^{-D}\int\int \mathbf{dp}_0\mathbf{dq}_0|\mathbf{p}_0\mathbf{q}_0\rangle\langle\mathbf{p}_0\mathbf{q}_0|. \tag{7}$$

Formally, the continuous phase space integrals introduced by Eq. (7) include the coherent states that are centered at all $(\mathbf{p}_0,\mathbf{q}_0)\subset\mathbf{R}^{2D}$ (this infinitely dense set of coherent states is labeled herein by $\mathcal{D}$). Numerical calculations, however, must evaluate such integrals by implementing MC or quadrature (i.e., discretization) techniques. In this paper we explore the implementation of an efficient discretization method.

The identity operator in a generic discrete nonorthogonal basis set $\{|i\rangle\}$ has the form,

$$\hat{1}=\sum_i\sum_j |i\rangle(\mathbf{S}^{-1})_{ij}\langle j|, \tag{8}$$

where $\mathbf{S}$ is the overlap matrix. Unfortunately, however, the numerical implementation of Eq. (8) is quite demanding since it requires inverting the overlap matrix, an operation with cost cubic in basis size. Therefore, in order to develop a numerically efficient discretization method we seek a subset of functions $|i\rangle$ that satisfy the relation,

$$\hat{1}=M^{-1}\sum_i |i\rangle\langle i|, \tag{9}$$

where $M>0$ is a normalization factor. Clearly, the operator (9) would be preferred over Eq. (8), as its application to a single function scales linearly with the size of the basis. In the algorithm we detail below, we apply this operator to a

superposition of $\approx N$ CS functions, yielding $\approx N^2$ scaling, still substantially more favorable than the N^3 scaling of Eq. (8).

Picking a set of functions $|i\rangle$ that satisfies Eq. (9) is not trivial. Such a set is called a *tight frame*,[57] and the study of such sets forms an active area of research in mathematics. It is important to notice that according to Eq. (7) the continuum set $\mathcal{D}$ forms a tight frame. This fact is used implictly in constructing the usual form of the HK propagator without the inverse overlap matrix by using a MC selection of the subset $|i\rangle$. Unfortunately, however, there is no discretization of $\mathcal{D}$ that formally yields a tight frame. If a particular set of functions that do not form a tight frame is used (i.e., *any* discrete set of CSs), the operator (8) must in theory be used. It is nonetheless possible to find discretizations that do satisfy Eq. (9) well enough for numerical calculations, and we present one here.

In order to describe discretizations that are both accurate and efficient we first consider the completeness of discrete CS basis sets. It has been shown[58] that the so-called von Neumann set[59] defined by the spacings

$$\Delta q = a/\sqrt{L}, \qquad \Delta p = 2\pi\hbar/a\sqrt{L}, \tag{10}$$

with $L=1$ and a an arbitrary constant, is the sparsest distribution of CS that forms a complete representation. The von Neumann set does not form a tight frame [i.e., Eq. (9) is not satisfied], as noted by other authors.[57,60,61] Making L sufficiently large, however, generates a discrete set that is numerically equivalent to a tight-frame since it approaches the set $\mathcal{D}$.

In this paper we implement instead a discretization of the basis defined by the spacings,

$$\Delta q \leqslant \tfrac{1}{2}\gamma^{-1/2}, \qquad \Delta p \leqslant \hbar\gamma^{1/2}. \tag{11}$$

We use this spacing because it defines, to double-precision accuracy, a tight frame [i.e., it satisfies Eq. (9) to double-precision accuracy]. A dilation of this spacing would reduce the accuracy of this approximation. A justification for this claim is given in Appendix A. Notice that here we have separate requirements on Δp and Δq (in contrast to the von Neumann set which stipulates a requirement on the product $\Delta p \Delta q = 2\pi\hbar$). The maximum spacings for Δq and Δp are equal to the uncertainty widths $\sqrt{\langle x\rangle^2 - \langle x^2\rangle}$ and $\sqrt{\langle p\rangle^2 - \langle p^2\rangle}$ taken over the CS introduced by Eq. (5), and the normalization constant $M = \Delta p \Delta q/(2\pi\hbar)$. The set of functions defined by such grid spacing is labeled by $\mathcal{F}$. In higher dimensions, the analogous set is defined by a direct product of the spacings given in Eq. (11). We emphasize that using the spacings given in Eq. (11) eliminates the need to calculate the inverse overlap matrix in the discrete representation of the identity operator. This is the primary reason for the relative efficiency of the approach implemented in this paper.

Using this particular set of functions we are ready to embark on a practical implementation of the time-slicing procedure introduced by Eq. (3). The procedure for propagating the wave function can be described by the following steps:

(1) Project the wave function $|\psi(t)\rangle$ ($t=0$ initially) onto $\mathcal{F}$, keeping all CS $|\mathbf{p}_j\mathbf{q}_j\rangle$ of $\mathcal{F}$ for which the expansion coefficient $|\langle \mathbf{p}_j\mathbf{q}_j|\psi(t)\rangle| \geqslant \zeta$, thereby defining a truncation of the infinite set $\mathcal{F}$ to a finite subset $\mathcal{F}'(t)$. Here, we assume that the resulting truncated basis set gives a sufficiently good representation of unity as defined by Eq. (9). Note that although $\mathcal{F}$ is defined according to regularly spaced basis functions, the truncation condition avoids the need for propagating the complete grid of coherent states by keeping only those basis functions that significantly overlap with $|\psi(t)\rangle$.

(2) Propagate the CS in $\mathcal{F}'(t)$ for a short time τ using the usual classical equations of motion. The CS will undergo classical flow in phase space to define the wave function $|\psi(t+\tau)\rangle$ via expansion in a new (irregularly spaced) set $\mathcal{F}'(t+\tau)$,

$$|\psi(t+\tau)\rangle = \int\int \mathbf{dp}_t \mathbf{dq}_t |\mathbf{p}_{t+\tau}\mathbf{q}_{t+\tau}\rangle C(\mathbf{p}_t\mathbf{q}_t,\tau) \times e^{iS(\mathbf{p}_t\mathbf{q}t,\tau)/\hbar}\langle \mathbf{p}_t\mathbf{q}_t|\psi(t)\rangle. \tag{12}$$

(3) Go to step (1), replacing $|\psi(t)\rangle$ with $|\psi(t+\tau)\rangle$.

The parameters ζ and τ are determined by the accuracy desired; decreasing the cutoff ζ and the time-slicing interval τ increases the accuracy of the algorithm. As $\zeta \to 0$ and $\tau \to 0$, the procedure is formally and numerically equivalent to a full quantum propagation scheme.

Typically, updating the representation by projecting the time evolved wave function onto $\mathcal{F}$ is the most time-consuming part of the procedure outlined above. We have developed an iterative method for efficiently performing the projection and outline the steps in Appendix B. The truncation $\mathcal{F} \to \mathcal{F}'(t)$ results in a basis set size that fluctuates in time according to the phase-space localization of the system at time t. This gives us the minimal possible representation in the CS grid basis at all times. We also note that, because of the redundancy in the set $\mathcal{F}$ and the smoothness of the CS functions, this representation actually achieves an accuracy in the wave function several orders of magnitude better than ζ.

There are three caveats worth mentioning. First, since the HK propagator does not conserve the norm, the result of the TSHK propagation may need to be renormalized at any desired time. All of the results presented in this paper were renormalized to unity. Second, one cannot let $\tau \to \infty$ when using an initial basis set $\mathcal{F}'$ and achieve the same numerical result as the usual HK procedure using a dense MC-sampled initial basis set. To achieve convergence with the HK propagator at long times it is necessary to use a very dense initial phase space sampling. Third, because the time-slicing procedure requires coupling of information among trajectories, parallel implementation of the TSHK algorithm is more complicated that for the simple independent trajectories of the usual HK method.

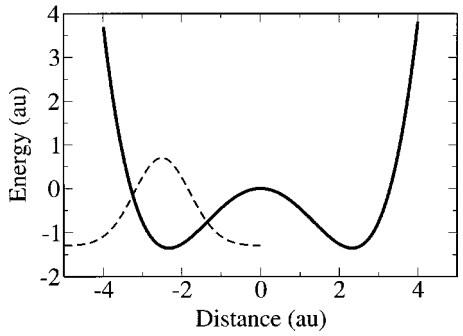

FIG. 1. The one-dimensional double-well model. (Solid) The potential given by Eq. (13). (Dotted) $|\psi|^2$ for the initial wave function given by Eq. (14).

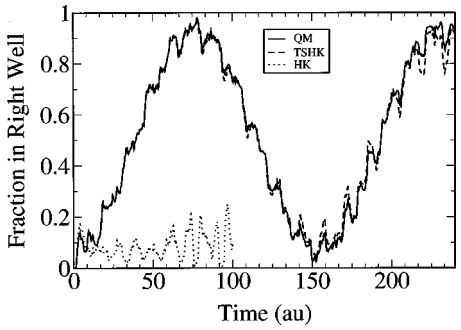

FIG. 2. Results of the one-dimensional double-well tests. The fraction of the total probability on the right half of the potential shown in Fig. 1. The solid line is the QM result. The failure of the HK method for this case is obvious from the dotted line. For clarity, only short-time HK results are given. The HK result is difficult to converge for long time. The TSHK results agree with the QM results for all times.

III. ONE- AND TWO-DIMENSIONAL DOUBLE-WELL MODELS

This section tests the capabilities of the time-sliced Herman–Kluk (TSHK) methodology, described in Sec. II, as applied to the description of tunneling dynamics in one- and two-dimensional double-wells. These model systems are especially challenging since they have so far defied even the most accurate SC-IVR techniques, including the standard implementation of the HK SC-IVR method.

A. One-dimensional double-well

In this section we examine the one-dimensional double-well model system described by the following Hamiltonian:

$$H(x,p)=\frac{p^2}{2m}+\frac{1}{16\eta}x^4-\frac{1}{2}x^2, \tag{13}$$

where $m=1$ a.u., and $\eta=1.3544$ a.u.

We examine the dynamics of the system by propagating a wavepacket $\psi_t(x)$ that is initially centered at $x_0=-2.5$ a.u.,

$$\psi_0(x)=\pi^{-1/4}\exp(-\tfrac{1}{2}[x-x_0]^2). \tag{14}$$

The system is schematically shown in Fig. 1.

The time dependent probability $P(t)$ of being on the right of the dividing surface located at $x=0$ is

$$P(t)=\langle\psi_t|h|\psi_t\rangle, \tag{15}$$

where the step function $h=1$ for $x>0$, and 0 otherwise. Figure 2 shows the evolution of $P(t)$ as a function of time. The final time ($t=240$ a.u.) represents about 60 vibrational periods for a state that oscillates in the bottom of one of the wells. The TSHK results were generated using a cutoff parameter $\zeta=10^{-4}$ and a CS width $\gamma=1.0$, resulting in a basis set of about 525 ± 50 coherent states. It is important to note that the size of the basis set fluctuates in time but its mean value remains approximately constant after an initial increase. A time-slicing interval $\tau=0.25$ a.u. was used for this system. For comparison, the time step used to integrate the HK equations of motion between each time-slice was 0.01 a.u.

The results obtained according to the standard implementation of the HK SC-IVR employed 8000 trajectories and a CS width $\gamma=0.5$. For clarity, HK results are shown in Fig. 1 for only moderate times. The HK results are increasingly difficult to converge for times longer than 100 a.u. The exact QM results were generated by implementing a Fourier transform grid-based method.[62]

The comparison presented in Fig. 1 shows that the TSHK results agree quantitatively with the full QM results. These results are converged with respect to reduction of the cutoff parameter ζ. The time-slicing interval of $\tau=0.25$ a.u. was necessary to achieve agreement over the whole range of time shown in Fig. 2. However, for moderate times (i.e., up to about 100 a.u.) it would have been sufficient to use a time-slicing interval $\tau\approx1$ a.u.

B. Two-dimensional double-well

The two-dimensional model system explored in this section is described by the following Hamiltonian:

$$H(\mathbf{x},\mathbf{p})=\frac{\mathbf{p}^2}{2m}+\frac{1}{16\eta}x_1^4-\frac{1}{2}x_1^2+\frac{1}{2}x_2^2+\frac{1}{20}x_1x_2, \tag{16}$$

where $m=1$ a.u., and $\eta=1.3544$ a.u. This system has been constructed by bilinearly coupling the one-dimensional double-well model system, described in Sec. III A, to a single harmonic oscillator.

The initial state is defined according to

$$\psi_0(\mathbf{x})=\pi^{-1/2}\exp(-\tfrac{1}{2}[x_1-x_0]^2-\tfrac{1}{2}x_2^2), \tag{17}$$

where $x_0=-2.5$ a.u.

In this example, we calculate the correlation functions,[74]

$$C_L(t)=\langle\phi_L|\psi(t)\rangle, \tag{18}$$

$$C_R(t)=\langle\phi_R|\psi(t)\rangle, \tag{19}$$

where $\phi_L=\psi_0$ and ϕ_R is the ''mirror image'' of ϕ_L reflected through the origin,

$$\phi_R(x_1,x_2)=\pi^{-1/2}\exp[-0.5(x_1-2.5)^2]\exp[-0.5x_2^2]. \tag{20}$$

Note that the correlation function $C_R(t)$ describes qualitatively the portion of the wavefunction that has tunneled from the left-hand side of the potential barrier to the right-hand side. The computed correlation functions are shown in Fig. 3.

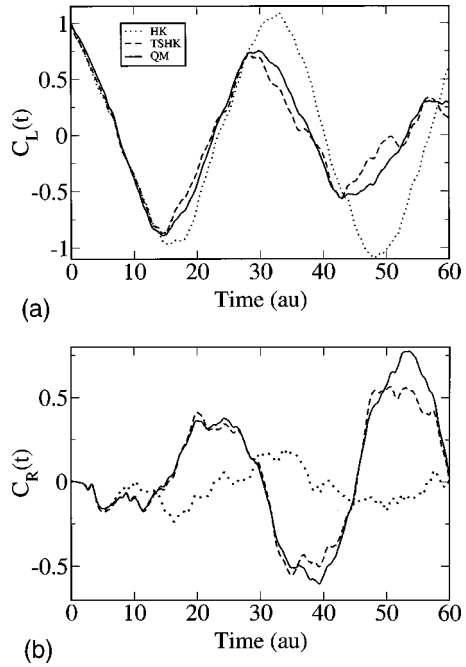

FIG. 3. Results of the two-dimensional double-well tests: (a) $C_L(t)$; (b) $C_R(t)$. The correlation functions are defined in the text, and $C_R(t)$ provides an indication of the wave packet tunneling into the right-hand well. The accuracy of the TSHK method is shown by the agreement between the solid and dashed lines. The HK method, shown by the dotted–dashed line, does not reproduce QM tunneling accurately.

The results obtained by implementing the TSHK approach were generated using a cutoff parameter $\zeta = 8 \times 10^{-3}$, a time-slicing interval of $\tau = 0.5$ a.u., and a CS width $\gamma = 1.0$. These parameters yield a basis set size of roughly $18\,000 \pm 1000$.

The results obtained according to the standard implementation of the HK SC-IVR were generated by propagating 16 000 trajectories, using the first-order Filinov filtering expression.[17,24,29,63] Specifically, we have implemented Eq. (13) of Ref. 63, setting $\epsilon = 10^{-6}$.[75] The CS width $\gamma = 0.5$. The QM results were obtained by implementing a split-operator propagation scheme[64] in conjunction with Fourier derivative techniques.

Figure 3 shows that the standard implementation of the HK SC-IVR approach is able to reproduce exact QM results but only for fairly short times. In contrast, the TSHK method is able to reproduce quantitatively full QM result up to moderate times, and give a good qualitative description for longer propagation times. Better agreement at longer times could always be obtained simply by further tightening the parameters ζ and τ.

IV. PROPAGATION ON COUPLED POTENTIAL ENERGY SURFACES

The TSHK method also provides a convenient way to perform wave packet calculations on coupled potential energy surfaces (e.g., electronically nonadiabatic dynamics). For the case of two coupled potential energy surfaces, the total system can be described by the Hamiltonian,

$$\hat{H} = \begin{pmatrix} \hat{H}_1 & \hat{V}_c \\ \hat{V}_c & \hat{H}_2 \end{pmatrix}, \tag{21}$$

where H_1 and H_2 are the adiabatic Hamiltonians on each surface and V_c is the coupling between them. The result of short time propagation of this system can be written as

$$\begin{aligned} |\psi_1(t+\tau)\rangle &= e^{i\hat{H}_1 \tau/\hbar} |\psi_1(t)\rangle - \frac{i\tau}{\hbar} \hat{V}_c |\psi_2(t)\rangle, \\ |\psi_2(t+\tau)\rangle &= e^{i\hat{H}_2 \tau/\hbar} |\psi_2(t)\rangle - \frac{i\tau}{\hbar} \hat{V}_c |\psi_1(t)\rangle, \end{aligned} \tag{22}$$

where ψ_1 and ψ_2 refer to the wave functions on the two potential surfaces. We can interpret these equations as having two steps: an adiabatic propagation on each surface (the first term on the right-hand side) followed by ''spawning'' of trajectories in which the coupling between the surface causes CSs on one surface to create new CSs on the other surface (the second term). When $\hat{V}_c$ can be written as a sum of Gaussians, the CSs spawned by the last term in Eq. (22) are available analytically.

One time step of our algorithm consists of adiabatically propagating each wave function on its diabatic surface using the HK propagator, adding to it the spawned CSs from the other surface, and re-expanding the resulting sum using the grid of CSs as in the single-surface problems. We apply this algorithm to one of the dual curve crossing models suggested by Tully[65] to test nonadiabatic dynamics. The model is described in the diabatic basis by

$$\begin{aligned} \hat{V}_1(q) &= 0, \\ \hat{V}_2(q) &= -0.1 \exp(-0.28q^2) + 0.05, \\ \hat{V}_c(q) &= 0.015 \exp(-0.06q^2). \end{aligned} \tag{23}$$

This model is widely used in tests of nonadiabatic dynamics, and we refer the reader to Ref. 65 for a depiction of the system.

The initial wave packets, representing a particle of mass 2000 a.u. begin to the left of the coupling region and propagate to the right. The specific initial conditions are identical to those of Ref. 65. We have employed a cutoff parameter $\zeta = 10^{-4}$ and a CS width $\gamma = 1.0$, which typically keep the size of the basis well below 1000 basis functions. We used time steps ranging from 0.025 a.u. (high initial momentum) to 0.1 a.u. (low initial momentum) for propagating the classical trajectories. By virtue of re-expanding the total wave function (adiabatic plus nonadiabatically spawned CSs) at each time step, our effective time-slicing interval is equal to the time step used for integrating the classical equations of motion. It would be possible to use a higher-order finite difference formula for $d\psi/dt$ to give a more accurate (though more complicated) expression for the nonadiabatically spawned CS portion of Eq. (22). This might enable a longer time interval between spawning and recombining events than the time needed to integrate the semiclassical (single-surface) propagator.

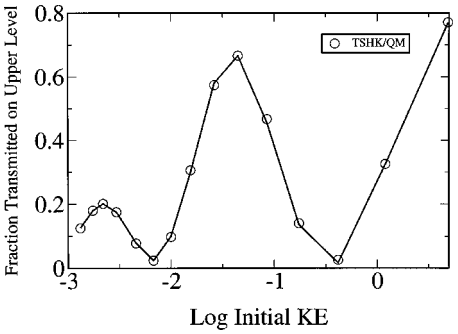

FIG. 4. The results of the nonadiabatic tests. The TSHK and QM results are given by the circles and are indistinguishable on the scale of the graph. The lines are drawn to guide the eye.

The performance of our method is measured by examining the total fraction of the initial wavepacket that is transmitted onto the second surface, as shown in Fig. 4. Our results agree quantitatively with the QM results generated by traditional methods.[65]

For a scattering system like this one, individual CSs may be discarded as they reach asymptotic regions and cause the wave function to become diffuse at long times.

V. DISCUSSION

The TSHK method is able to reproduce quantitatively full QM results describing tunneling dynamics in one- and two-dimensional double-well systems. This is not a surprise because the method is designed to approach exact QM calculations both formally and numerically. Previous real-time path-integral simulations have been limited to one-dimensional systems, and thus the results of Sec. III B are notable, as they constitute exact path integral results from a general two-dimensional potential. The fact that our method is derived from repeated applications of a path-integral propagator has the benefit that the system under study could be coupled to a bath of oscillators using an influence functional formalism,[66] a technique that is not available for direct grid-based solution of the time-dependent Schrödinger equation. Such a method would allow us to examine two-dimensional systems coupled to a bath, extending the capabilities of previous computational studies that were limited to one-dimensional model systems.[67]

The ability of our method to describe two-dimensional systems is due to the compact nature of the CS representation and not restricted to a specific SC-IVR propagator (e.g., the HK SC-IVR). The only requirement is that the short-time propagation should map CSs onto functions that can themselves be projected analytically onto other CSs. This requirement thus includes a large class of approximate semiclassical and QM methods. In particular, we have tested the WKB approximate prefactor,[19]

$$C_\tau(\mathbf{p}_0,\mathbf{q}_0)=\sqrt{\det[\mathbf{M}_t]}, \tag{24}$$

with

$$\det(\mathbf{M}_t)=\prod_{k=1}^{N}\frac{1}{2}\left(\sqrt{\frac{\omega_0(k)}{\omega_t(k)}}+\sqrt{\frac{\omega_t(k)}{\omega_0(k)}}\right)\times\cos\left(\int_0^t dt'\,\omega_{t'}(k)\right)-\frac{i}{2}\left(\frac{2\hbar\gamma(k)}{\sqrt{\omega_0(k)\omega_t(k)}}+\frac{\sqrt{\omega_0(k)\omega_t(k)}}{2\hbar\gamma(k)}\right)\sin\left(\int_0^t dt'\,\omega_{t'}(k)\right), \tag{25}$$

and we have found that it works well when implemented according to the TSHK approach. This prefactor requires keeping track of the evolution of the instantaneous eigenfrequencies $\omega_t(k)$, but avoids the need of propagating monodromy matrix elements. In contrast, the simple frozen Gaussian technique originally discussed by Heller,[68] in which the prefactor remains equal to unity at all times, is not accurate enough to be implemented with the time-slice intervals used in this work.

It is worthwhile to compare our method to others in the literature. As was mentioned in the introduction, the time-slicing idea has already been considered within the context of semiclassical techniques. In fact, Heller proposed a similar approach as early as 1975,[69] though with a different short-time propagator and without making reference to the strict requirements on the basis of coherent states (not surprisingly, as the theory of CS frames was not developed until the mid-1980s). However, there are no numerical examples of this "wave packet path integral" method in the literature. Concatenation of short-time semiclassical propagators is also central to the so-called hybrid mechanics method.[60,70] The resolution of identity used in that work, however, involves an inverse overlap matrix calculated by singular value decomposition, and does not dynamically optimize the basis set as a function of time. Andersson,[61] while noting the concept of tight frames but not employing them explicitly, has taken the hybrid mechanics method one step further by implementing an iterative calculation of the inverse overlap matrix, which may scale as less than N^3 if sparse matrix techniques are employed. Recently, Grossmann provided an application[55] of a "time-sliced" HK propagation scheme (with only two time-slices), to a one-dimensional scattering example. His work implemented a MC evaluation of the identity operator, introduced by Eq. (7). The results, while an improvement over regular HK, did not agree exactly with full quantum mechanical calculations.

Clearly, a generalization to higher dimensions would be a valuable tool, permitting direct path integral simulation of more realistic models of chemical systems. Because of the overall N^2 scaling of the TSHK method, systems with large basis sets pose a problem. The use of direct-product CS grids scales poorly with dimensionality, and would greatly increase the number of basis functions need for three-dimensional and larger systems. Such calculations might therefore be very computationally challenging. Monte Carlo importance sampling methods are usually the most efficient computational techniques for calculating high dimensional integrals. In the context of the TSHK method, the MC technique would entail construction of a tight frame with randomly spaced CS basis functions. This work is however the

subject of current ongoing research in our group. While the grid-based approach is simple, accurate, and efficient enough for up to two dimensions, there might be more efficient ways of constructing basis sets in higher dimensionality.

VI. CONCLUSIONS

We have shown in this paper how to extend the capabilities of the HK SC-IVR method to describe accurately tunneling between disjoint classically allowed regions, as well as long-time dynamics. We have shown that this can be accomplished by implementing the HK SC-IVR in conjunction with a time-slicing technique in a discrete coherent state representation. We have demonstrated that the time-sliced HK propagator accurately describes tunneling dynamics in one- and two-dimensional double-well model systems for propagation times that correspond to more than 60 vibrational periods at the bottom of one of the wells. We have shown that the methodology can also be directly implemented to describe nonadiabatic dynamics on coupled potential energy surfaces. Quantitative agreement with full quantum mechanical calculations was achieved for all model systems investigated. Furthermore, we have discussed the representation of the identity operator in a discrete CS basis. We have demonstrated that such a representation can be sufficiently compact as to avoid the need for calculating the inverse overlap matrix. The insight gained into the discrete CS representation suggests that straightforward application of the time slicing technique to three-dimensional systems might be computationally quite demanding. Nonetheless, we are optimistic about the utility of the method for describing adiabatic and nonadiabatic dynamics in systems that are more complex than those previously investigated with other path integral techniques.

ACKNOWLEDGMENTS

J.C.B. would like to thank Professor John Tully for support and encouragement, as well as helpful suggestions. J.C.B. has been supported by a DoD graduate fellowship during the undertaking of this work. Additional support was provided by the National Science Foundation Grant No. CHE-0075744. V.S.B. acknowledges financial support for this work from the Provost's office at Yale University and a generous allocation of supercomputer time from the National Energy Research Scientific Computing Center.

APPENDIX A: DISCRETIZATION SCHEME

This Appendix shows how to obtain the discretization scheme, introduced by Eq. (11). We explore a basis set of coherent states,

$$\langle x|p_m q_n\rangle = \left(\frac{2\gamma}{\pi}\right)^{-1/4} \exp[-\gamma(x-q_n)^2 + i p_m (x-q_n)], \tag{A1}$$

for which the basis functions are centered at grid points,

$$\begin{aligned} p_m &= p_0 + m\Delta p, \\ q_n &= q_0 + n\Delta q, \end{aligned} \tag{A2}$$

where the spacings in coordinates and momenta are Δq and Δp, respectively. The goal is to estimate how well such a representation approximates a tight frame, i.e., how well an arbitrary L^2 function is approximated by the following expression:

$$|f\rangle \approx M^{-1} \sum_{m,n} |p_m q_n\rangle\langle p_m q_n|f\rangle. \tag{A3}$$

It is well known that, according to the Klauder identity (7), any such function $f(x)$ can be expanded in the continuous CS representation,

$$|f\rangle = \frac{1}{2\pi\hbar} \int\int dp'\,dq'\,|p'q'\rangle\langle p'q'|f\rangle. \tag{A4}$$

Therefore, as an estimate, we explore how well any arbitrary basis function $|p'q'\rangle$ can be represented by the expansion introduced by Eq. (A3). In particular, we will explore the discretization,

$$\begin{aligned} \Delta q &= \lambda_q / 2\gamma^{-1/2}, \\ \Delta p &= \lambda_p \hbar\, \gamma^{1/2}, \end{aligned} \tag{A5}$$

where λ_p and λ_q are adjustable parameters. When $\lambda_p = \lambda_q = 1$, the spacings Δp and Δq correspond to the critical grid spacings introduced by Eq. (11).

We examine the quantity,

$$1 = \langle p'q'|p'q'\rangle \approx M^{-1} \sum_{m,n} \langle p'q'|p_m q_n\rangle\langle p_m q_n|p'q'\rangle, \tag{A6}$$

since the better the grid representation is, the closer the sum above will approximate 1. The summation can be written as

$$\begin{aligned} & M^{-1} \sum_{m,n} |\langle p_m q_n|p'q'\rangle|^2 \\ &= M^{-1} \left| \sum_{m,n} \exp\left[-\frac{\gamma}{2}(q_0 + n\Delta q - q')^2\right] \right. \\ &\quad \times \exp\left[-\frac{1}{8\gamma\hbar^2}(p_0 + m\Delta p - p')^2\right] \exp\left[\frac{i}{\hbar}\{(p' - p_0 \right. \\ &\quad \left. \left. - m\Delta p) + p'q' - (p_0 + m\Delta p)(q_0 + n\Delta q)\}\right] \right|^2 \\ &= M^{-1} \sum_{m,n} \exp[-\gamma(q_0 + n\Delta q - q')^2] \\ &\quad \times \exp\left[-\frac{1}{4\gamma\hbar^2}(p_0 + m\Delta p - p')^2\right] \\ &= M^{-1} \exp[-\gamma(q_0 - q')^2] \exp\left[-\frac{1}{4\gamma\hbar^2}(p_0 - p')^2\right] \\ &\quad \times \left\{ \sum_n \exp[-2\gamma n(q_0 - q')\Delta q] \exp[-\gamma \Delta q^2 n^2] \right\} \\ &\quad \times \left\{ \sum_m \exp\left[-\frac{1}{2\gamma\hbar^2} m(p_0 - p')\Delta p\right] \right. \\ &\quad \left. \times \exp\left[-\frac{1}{4\gamma\hbar^2}\Delta p^2 m^2\right] \right\}. \end{aligned} \tag{A7}$$

TABLE I. Accuracy of tight frame identity operator.

λ_q	$\delta(\lambda_q)$
0.8	2.88(−26)
0.9	1.07(−20)
1.0	6.66(−16)
1.1	8.72(−14)
1.2	1.47(−11)
1.3	7.81(−10)
1.4	1.81(−9)
1.5	2.27(−7)
1.6	1.78(−6)
1.7	9.74(−6)
1.8	4.02(−5)
1.9	1.33(−4)
2.0	3.67(−4)
2.1	8.74(−4)
2.2	1.85(−3)
2.3	3.54(−3)

The two sums in curly brackets, which are known as the Jacobi theta functions θ_3, can both be written in the form,

$$\sum_n \exp\left[-\alpha\left(n+\frac{\beta}{2}\right)^2\right]\exp[\alpha\beta^2/2]. \tag{A8}$$

Examining the sum over n, for which $\alpha=\gamma\Delta q^2$ and $\beta=2(q_0-q')/\Delta q$, we find that

$$\exp[\alpha\beta^2/4]=\exp[\gamma(q_0-q')^2], \tag{A9}$$

which exactly cancels the factor $\exp[-\gamma(q_0-q')^2]$ in Eq. (A7). The offset in the exponent becomes $\beta/2=(q_0-q')/\Delta q$. Because the grid center q_0 can be chosen arbitrarily such that q' is close to q_0, we can restrict $|\beta|\leqslant 1$. Substituting $\alpha=\lambda_q^2/4$, the product of all q-dependent factors in Eq. (A7) is seen to be

$$\sum_n \exp\left[-\frac{\lambda_q^2}{4}\left(n+\frac{\beta}{2}\right)^2\right]. \tag{A10}$$

This sum is a regularly spaced quadrature of the Gaussian $\exp[-\lambda_q^2 n^2/4]$, with the quadrature points at some offset $\beta/2$ from the center of the Gaussian. A continuous integration over n would yield the number $\sqrt{4\pi/\lambda_q^2}$. The quadrature result will vary from this answer depending on the offset $\beta/2$. For λ_q large (a very peaked Gaussian), the location of the grid points changes the quadrature greatly, but for small λ_q it is relatively unimportant.

Recall that we are trying to pick grid spacing factors λ_q and λ_p such that the arbitrary CS $|p'q'\rangle$ is well-described by the CS grid representation. This means that we need to pick λ_q such that the sum (A10) does not depend significantly on β. We choose to quantify this dependence by looking at the difference in the sum for the two cases $\beta=0$ (no offset) and $\beta=1$ (maximum offset). We define the function

$$\delta(\lambda_q)=\left|\sum_n\left\{\exp\left[-\frac{\lambda_q^2}{4}n^2\right]-\exp\left[-\frac{\lambda_q^2}{4}\left(n+\frac{1}{2}\right)^2\right]\right\}\right| \tag{A11}$$

in order to examine the effect of varying λ_q. We have tabulated the values of $\delta(\lambda_q)$ for a range of λ_q and present the results in Table I. The p-dependent terms in Eq. (A7) can be treated in a manner identical to the q-dependent ones.

Examining the data in Table I, we see that choosing $\lambda_q=\lambda_p=1$ gives double precision accuracy, and hence this is the value we use in normal computation. Recall that the tight frame identity operator, introduced by Eq. (9), is used repeatedly so that any error in the expansion will compound rapidly as the propagation progresses. A slight dilation in the grid spacing would not yield any significant savings in computational time, and our tests with dilations on the order of $\lambda_q\approx 2$, $\lambda_p\approx 2$ have given qualitatively incorrect answers.

Finally, carrying through the integration-limit answer for the sums over n and m in Eq. (A7) implies a normalization,

$$M^{-1}=\frac{\Delta p\Delta q}{2\pi\hbar} \tag{A12}$$

as one might expect from a naive discretization of Eq. (7).

APPENDIX B: IMPLEMENTATION METHOD

This Appendix outlines an efficient method of projecting a wavefunction composed of a linear combination of arbitrary spaced CSs onto a minimal grid of equally spaced CSs to create the set $\mathcal{F}'$.

We will call the set of arbitrarily spaced CSs A:

(1) Define the center of the new grid (Q_0,P_0) (we use capital letters to avoid confusion with notation elsewhere in the paper). We use the arithmetic average of the phase space centers of all the CSs in A.
This defines implicitly all the grid points $(Q_{ij\cdots}=i\Delta Q_1\hat{Q}_1+j\Delta Q_2\hat{Q}_2+\cdots, P_{kl\cdots}=k\Delta P_1\hat{P}_1+l\Delta P_2\hat{P}_2)$.
Set iteration counter $n=0$.
Initialize the new set of CSs $\mathcal{F}'$ as the empty set.
Initialize a set of known negligible CSs N as the empty set. Initiate sets T and K as the empty set.
(2) For each CS in A, add the grid point closest to this CS to a list of test grid points $T^{(0)}$.
(3) Project the CS $|b\rangle$ centered at each grid point b in $T^{(n)}$ onto the current wave function, defining $c=|\langle b|\psi\rangle|$.
If $c>\zeta$, add the grid point b to the set $K^{(n)}$.
Otherwise, add the grid point b to the list of known negligible grid points N.
(4) Add the grid points in set $K^{(n)}$ to the set $\mathcal{F}'$. Sort $\mathcal{F}'$ and N for easy searching in the next step.
(5) Build a new list of test grid points $T^{(n+1)}$ consisting of all nearest neighbor grid points to those in the set $K^{(n)}$, eliminating known neglible grid points and those already in $\mathcal{F}'$.
(6) If the set $T^{(n+1)}$ is not empty, increment $n\rightarrow n+1$ and go to Step 3. Otherwise, $\mathcal{F}'$ is complete.

We use an integer array variable $(i,j,\ldots,k,l,\ldots)$ to refer to each grid point. This enables efficient sorting and searching for duplicate and known negligible grid points. Sorting and searching is a trivial computational task. The majority of computer time used is spent in step (3).

[1] M. F. Herman and E. Kluk, Chem. Phys. **91**, 27 (1984).
[2] W. H. Miller, J. Chem. Phys. **53**, 3578 (1970).

[3] W. H. Miller, J. Phys. Chem. A **105**, 2942 (2001).
[4] R. Gelabert, X. Giménez, M. Thoss, H. Wang, and W. H. Miller, J. Chem. Phys. **114**, 2572 (2001).
[5] X. Sun and W. H. Miller, J. Chem. Phys. **106**, 916 (1997).
[6] G. Campolieti and P. Brumer, Phys. Rev. A **50**, 997 (1994).
[7] G. Campolieti and P. Brumer, J. Chem. Phys. **96**, 5969 (1992).
[8] G. Campolieti and P. Brumer, J. Chem. Phys. **107**, 791 (1997).
[9] A. R. Walton and D. E. Manolopoulos, Mol. Phys. **87**, 961 (1996).
[10] M. F. Herman, Chem. Phys. Lett. **275**, 445 (1997).
[11] K. G. Kay, J. Chem. Phys. **100**, 4377 (1994).
[12] K. G. Kay, J. Chem. Phys. **100**, 4432 (1994).
[13] K. G. Kay, J. Chem. Phys. **101**, 2250 (1994).
[14] M. L. Brewer, J. S. Hulme, and D. E. Manolopoulos, J. Chem. Phys. **106**, 4832 (1997).
[15] M. Ovchinnikov and V. A. Apkarian, J. Chem. Phys. **108**, 2277 (1998).
[16] X. Sun and W. H. Miller, J. Chem. Phys. **108**, 8870 (1998).
[17] V. S. Batista and W. H. Miller, J. Chem. Phys. **108**, 498 (1998).
[18] V. S. Batista, M. T. Zanni, B. J. Greenblatt, D. M. Neumark, and W. H. Miller, J. Chem. Phys. **110**, 3736 (1999).
[19] V. Guallar, V. S. Batista, and W. H. Miller, J. Chem. Phys. **110**, 9922 (1999).
[20] V. Guallar, V. S. Batista, and W. H. Miller, J. Chem. Phys. **113**, 9510 (2000).
[21] V. S. Batista and P. Brumer, J. Phys. Chem. A **105**, 2591 (2001).
[22] V. S. Batista and P. Brumer, J. Chem. Phys. **114**, 10321 (2001).
[23] K. G. Kay, J. Chem. Phys. **101**, 2250 (1994).
[24] V. S. Filinov, Nucl. Phys. B **271**, 717 (1986).
[25] N. Makri and W. H. Miller, Chem. Phys. Lett. **139**, 10 (1987).
[26] R. D. Coalson, D. L. Freeman, and J. D. Doll, J. Chem. Phys. **85**, 4567 (1986).
[27] B. W. Spath and W. H. Miller, J. Chem. Phys. **104**, 95 (1996).
[28] B. W. Spath and W. H. Miller, Chem. Phys. Lett. **262**, 484 (1996).
[29] B. E. Guerin and M. F. Herman, Chem. Phys. Lett. **286**, 361 (1998).
[30] H. Wang, D. Manolopoulos, and W. H. Miller, J. Chem. Phys. **115**, 6317 (2001).
[31] H. B. Wang, X. Sun, and W. H. Miller, J. Chem. Phys. **108**, 9726 (1998).
[32] E. Pollak and L. J. Liao, J. Chem. Phys. **108**, 2733 (1998).
[33] J. Shao, L. J. Liao, and E. Pollak, J. Chem. Phys. **108**, 9711 (1998).
[34] X. Sun, H. B. Wang, and W. H. Miller, J. Chem. Phys. **109**, 7064 (1998).
[35] N. Makri and K. Thompson, J. Chem. Phys. **110**, 1343 (1999).
[36] X. Sun and W. H. Miller, J. Chem. Phys. **110**, 6635 (1999).
[37] K. G. Kay, J. Chem. Phys. **110**, 8912 (1999).
[38] K. G. Kay, J. Chem. Phys. **107**, 2313 (1997).
[39] S. Garashchuk and D. Tannor, Chem. Phys. Lett. **262**, 477 (1996).
[40] V. A. Mandelshtam and M. Ovchinnikov, J. Chem. Phys. **108**, 9206 (1998).
[41] T. F. George and W. H. Miller, J. Chem. Phys. **57**, 2458 (1972).
[42] T. Uzer, D. Noid, and R. Marcus, J. Chem. Phys. **79**, 4412 (1983).
[43] R. Marcus and M. Coltrin, J. Chem. Phys. **67**, 2609 (1977).
[44] N. Makri and W. H. Miller, J. Chem. Phys. **91**, 4026 (1989).
[45] Y. Guo and D. Thompson, J. Chem. Phys. **105**, 1070 (1996).
[46] W. H. Miller, J. Chem. Phys. **95**, 9428 (1991).
[47] E. J. Heller, J. Chem. Phys. **95**, 9431 (1991).
[48] R. P. Feynman, Rev. Mod. Phys. **20**, 367 (1948).
[49] P. Pechukas, Phys. Rev. **191**, 166 (1969).
[50] W. H. Miller, Adv. Chem. Phys. **25**, 69 (1974).
[51] J. D. Doll, T. L. Beck, and D. L. Freeman, J. Chem. Phys. **89**, 5753 (1988).
[52] N. Makri, Comput. Phys. Commun. **63**, 389 (1991).
[53] E. Kluk, M. F. Herman, and H. L. Davis, J. Chem. Phys. **84**, 326 (1986).
[54] R. P. Feynman and Hibbs, *Quantum Mechanics and Path Integrals* (McGraw–Hill, New York, 1965).
[55] F. Grossmann, Phys. Rev. Lett. **85**, 903 (2000).
[56] J. R. Klauder, J. Math. Phys. **4**, 1058 (1963).
[57] I. Daubechies, A. Grossmann, and Y. Meyer, J. Math. Phys. **27**, 1271 (1986).
[58] A. M. Perelomov, Teor. Mat. Fiz. **6**, 213 (1971).
[59] J. von Neumann, *Mathematical Foundations of Quantum Mechanics* (Princeton University Press, Princeton, 1985).
[60] D. Huber and E. J. Heller, J. Chem. Phys. **89**, 4752 (1988).
[61] L. M. Andersson, J. Chem. Phys. **115**, 1158 (2001).
[62] D. Kosloff and R. Kosloff, J. Comput. Phys. **52**, 35 (1983).
[63] B. R. McQuarrie and P. Brumer, Chem. Phys. Lett. **319**, 27 (2000).
[64] J. A. Fleck, J. R. Morris, and M. D. Feit, Appl. Phys. **10**, 129 (1976).
[65] J. C. Tully, J. Chem. Phys. **93**, 1061 (1990).
[66] R. P. Feynman and F. L. Vernon, Jr., Ann. Phys. (N.Y.) **24**, 118 (1963).
[67] M. Topaler and N. Makri, J. Chem. Phys. **101**, 7500 (1994).
[68] E. J. Heller, J. Chem. Phys. **75**, 2923 (1981).
[69] E. J. Heller, Chem. Phys. Lett. **34**, 321 (1975).
[70] D. Huber, S. Ling, D. G. Imre, and E. J. Heller, J. Chem. Phys. **90**, 7317 (1989).
[71] D. J. Tannor and S. Garashchuk, Annu. Rev. Phys. Chem. **51**, 553 (2000).
[72] V. A. Mandelshtam, J. Chem. Phys. **108**, 9999 (1998).
[73] J. R. Reimers and E. J. Heller, J. Phys. Chem. **92**, 3225 (1988).
[74] These types of wave packet cross-correlation functions are common in scattering calculations (Ref. 71) and can be used at long times (or in conjunction with filter-diagonalization techniques (Ref. 72) at short times) to extract spectral properies such as eigenenergies and tunneling splittings. However, accurate reproduction of dynamical quantities like that seen here is a much more difficult task than reproducing spectral properties (Ref. 73), so we do not discuss this data.
[75] Note that the addition and multiplications in that equation need to be interchanged.